Conformational control via sequence for a heteropeptoid in water: coupled NMR and Rosetta modelling

Trideep Rajale,‡[a] Jacob C. Miner,‡[b,c] Ryszard Michalczyk,[c] M. Lisa Phipps,[a] Jurgen G. Schmidt,[c] Robert D. Gilbertson,[d] Robert F. Williams,[c] Charlie E. M. Strauss,[*c] and Jennifer S. Martinez[*e,f]

Supplementary Information

[a]Center for Integrated Nanotechnologies, Los Alamos National Laboratory, Los Alamos, New Mexico 87545, United States.

[b]Theoretical Biology and Biophysics, Los Alamos National Laboratory, Los Alamos, New Mexico 87545, United States.

[c]Bioscience Division, Los Alamos National Laboratory, Los Alamos, New Mexico 87545, United States

[d]Materials Science and Technology Division, Los Alamos National Laboratory, Los Alamos, New Mexico 87545, United States.

[e]Center for Materials Interfaces in Research and Applications, Northern Arizona University, Flagstaff, Arizona 86011, United States.

[f]Department of Applied Physics and Materials Science, Northern Arizona University, Flagstaff, Arizona 86011, United States.

‡ These authors contributed equally

Corresponding Author

*E-mail: jennifer.martinez@nau.edu, cems@lanl.gov

Table of contents   **Page**

Experimental Details

General. All of the organic reagents and solvents were purchased from commercial sources and used without further purification. Fmoc-protected Rink amide resin (100-200 mesh, substitution 0.35 mmol/g) was purchased from Novabiochem. The conventional peptoid synthesis at room temperature was performed in a standard glass peptide-synthesis vessel (Chemglass). Microwave-assisted peptoid synthesis was carried out on an automated microwave synthesizer (Liberty Automated Microwave Peptide Synthesizer, CEM) equipped with a temperature probe for real time temperature monitoring. All swelling, deprotection and final cleavage steps were performed at room temperature in a 10-mL single frit polypropylene tube sealed with caps and stoppers. Analytical reverse-phase HPLC was performed using a Waters 600 HPLC with an attached 2767 Autosampler and a 2487 Detector operating at 215 nm with a C18 reverse-phase column (Gemini NX-C18 110 Å, 5 μm, 4.6 mm i.d. x 250 mm). Mobile phase: solvent A = 0.1% TFA in water and solvent B = 0.1% TFA in acetonitrile. The relative peak amounts were determined by integration at 215 nm and purity of the desired peptoid was computed. Semipreparative HPLC peptoid isolations were performed using reverse-phase C18 column (Gemini NX-C18 110 Å, 5 μm, 10 mm i.d. x 250 mm). Circular dichroism (CD) spectra were obtained on Chirascan CD spectrometer (Model q-CD Plus) from Applied Photophysics.

General procedure for a peptoid synthesis under microwave conditions. Automated microwave sequence for resin-loading, resin swelling, Fmoc-deprotection, acylation using N',N-diisopropylcarbodiimide (DIC) , and displacement steps was developed on the PepDriver tool for the CEM microwave peptide synthesis system.

Synthesis protocol:

CEM Liberty Automated Microwave Peptide Synthesizer

1. Synthesis Scale: 0.05 mmol
2. Resin: Fmoc-Rink Amide resin LL (0.35 mmol/g)
3. Deprotection: 20% 4-methylpiperidine in NMP; 3 min at 75 ^{o}C
4. Acylation: BrCH$_2$COOH/DIC (1.0/1.2 eq); 5 min at 30-40 ^{o}C
5. Displacement: submonomer (1.0 eq); 2 min at 50 ^{o}C, then 3 min at 75 ^{o}C

General procedure for a peptoid synthesis at room temperature. Fmoc-protected Rink amide resin (143 mg, 0.05 mmol) was transferred to a peptide glass vessel. Resin was rinsed with 2 x 2 mL dichloromethane and then swollen in DMF (2.5 mL) for 30 min. The DMF was drained and 20% piperidine/DMF (2 x 2.5 mL) was added for Fmoc-deprotection for 20 min each. After drainage the resin was washed with DMF (5 x 1.5

mL). Acylation was performed by adding 0.6 M Bromoacetic acid in NMP (1.25 mL) and 50% (v/v) DIC in NMP (0.3 mL) and agitated for 30 min. Then the resin beads were washed with NMP (5 x 2.5 mL). For the displacement step 1 M Amine (10 eq) in NMP (1.7 mL) was added and mixed for 1.5 hrs. The beads were then washed with NMP (5 x 2.5 mL) and the acylation-displacement sequence was repeated for the addition of the next amine residue. Note that a longer reaction time of 2 hrs was needed for the displacement step with the Ns1npe amine.

Peptoid Cleavage Protocols. At the end of the final amine addition the beads were transferred to a single frit polypropylene tube and washed with methylene chloride (5 x 2.5 mL). Dried beads were treated with the cleavage cocktail (95% TFA, 2.5% H_2O, 2.5% triisopropylsilane) and the mixture was agitated for 2 hrs. Solvents were evaporated over a stream of nitrogen and the crude product was precipitated by adding ice cold ether. The crude peptide was lyophilized and stored at −20 °C.

Peptoid Purification. Peptoid oligomers (**H1**-**H9**) were purified to >95% homogeneity by semi-preparative reverse-phase HPLC (gradient elution was 20-80% solvent B in 24 minutes). The solvent was removed *in vacuo* using a rotavap at 40 °C. Concentrated fractions were subjected to lyophilization and peptoids were isolated as white powders.

Purity Analyses. The samples were analyzed by HPLC, and purities were determined by integration at 215 nm as described above. A C18 column (Gemini NX-C18 110 Å, 4.6 x 250 mm) was used for analysis of all peptoid pentamers and octamers. Fractions containing the desired products were collected and analyzed by ESI mass spectral analysis.

CD Analyses. CD spectra were obtained in a square quartz cell (path length 0.1 cm on the Chirascan q-CD Plus Spectrometer) at room temperature using a scan rate of 100 nm/min, with five averaged scans per spectrum. Peptoid stock solutions were prepared immediately prior to CD analysis by dissolving ~1 mg of peptoid in 1 mL of 10 mM sodium phosphate buffer (pH 7.5 at 25 ºC). The stock solutions were diluted to the desired concentration (50 µM) using a calibrated micropipette.

NMR Characterization.
All NMR spectra were obtained on a Bruker AVANCE III NMR spectrometer operating at ^{1}H frequency of 700.13 MHz using standard pulse sequences from the Topspin software library. Data were collected on ~2 mM peptoid samples, prepared by dissolving in ~1 mg of peptoid in 1 mL of 10 mM phosphate buffer at pH 7.5 in 90%-H_2O/10%-D_2O. Data were processed and analyzed using MNova 12 software.

One-dimensional spectra were apodized with an exponential function corresponding to 1 Hz line broadening, zero filled to 2x data points and Fourier transformed. Baseline in the spectra was corrected using Whittaker smoother.

In 2D experiments, 2048 data points in f2 and 400 complex points in f1 were collected in each experiment. The data were linearly predicted to 512 complex points in f1, zero filled to a 2048x2048 matrix and apodized with a 90° shifted sine square function before Fourier transform. ^{1}H-^{1}H TOCSY spectra were collected with 40-ms and 60-ms mixing times; ROESY spectra were collected with mixing times from 100 to 400 ms.

NMR shows consistent methyl proton linewidths for all naphthyl protons (3 – 5 Hz). This is strongly suggestive of no self-association, as any aggregates would have higher molecular weight, and the NMR linewidths would have increased. Dynamics light scattering (DLS) of multiple peptoids did not show evidence of aggregation. See Supplemental Page 20 for details on analysis of NMR data.

Scheme S1. Sub-monomer synthesis for sequence-specific peptoids[1,2]

acylation: bromoacetic acid, DIC, NMP

displacement: amines, NMP

Sequence-specific peptoids

Figure S1. HPLC traces for peptoid **H5** synthesized via (A) microwave conditions and (B) conventional room-temperature route, with crude purities.
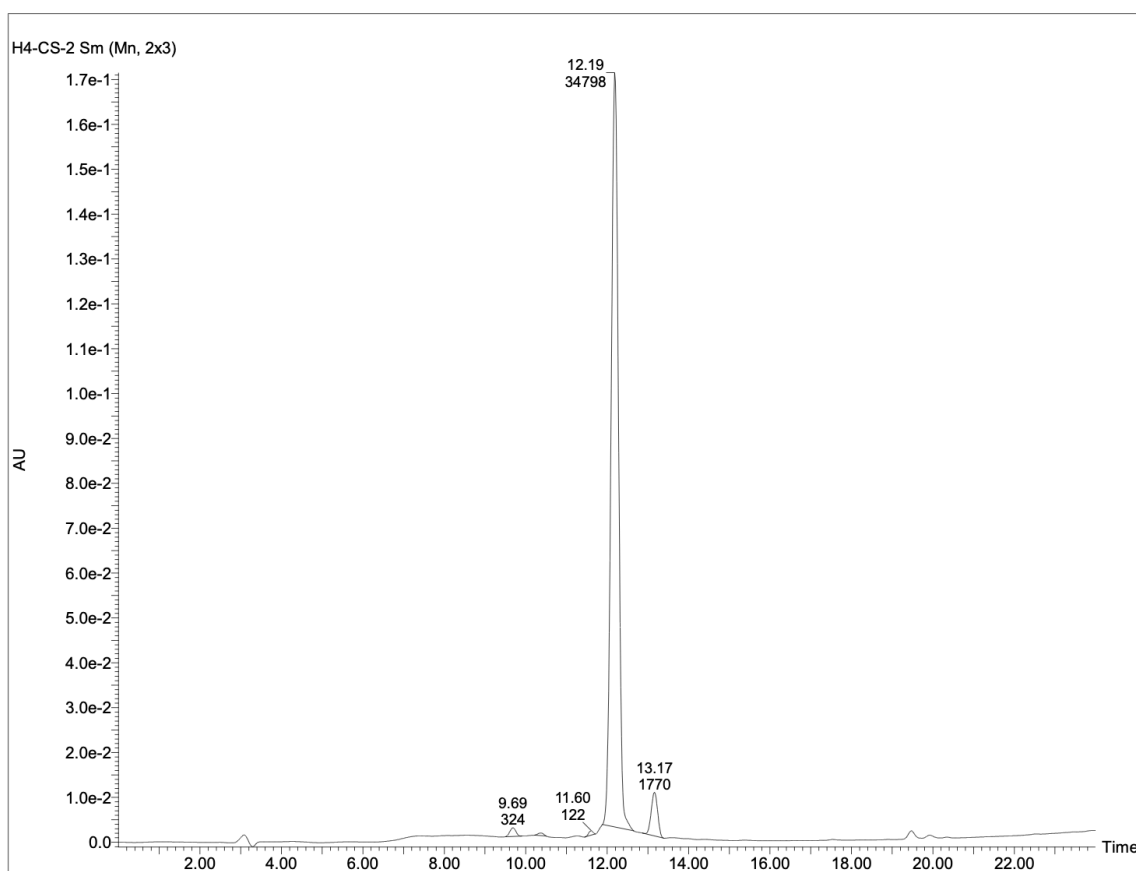
Figure S2. Analytical HPLC trace of naphthyl-containing peptoid (**H4**) following semi-preparative HPLC purification.

Table S1. Octamer sequences synthesized using microwave protocol[a]

entry	peptoid sequence[b]	MS[c]	purity (%)[d]
H8	H-Nspe-Nsce-Nme-Nspe-Nsce-Nme-Nspe-Nsce-NH$_2$	1118.2	68
H9	H-Nspe-Nae-Nme-Nspe-Nae-Nme-Nspe-Nae-NH$_2$	1031.3	62

[a]Peptoids were synthesized on Rink amide resin (0.05 mmol scale). [b]Nae amine as Boc-protected and Nsce amine as *tert*-butyl protected. [c]ESI-MS data. [d]Percent purity as estimated by analytical RP-HPLC of the crude dry peptoid sample after ether precipitation and washing.
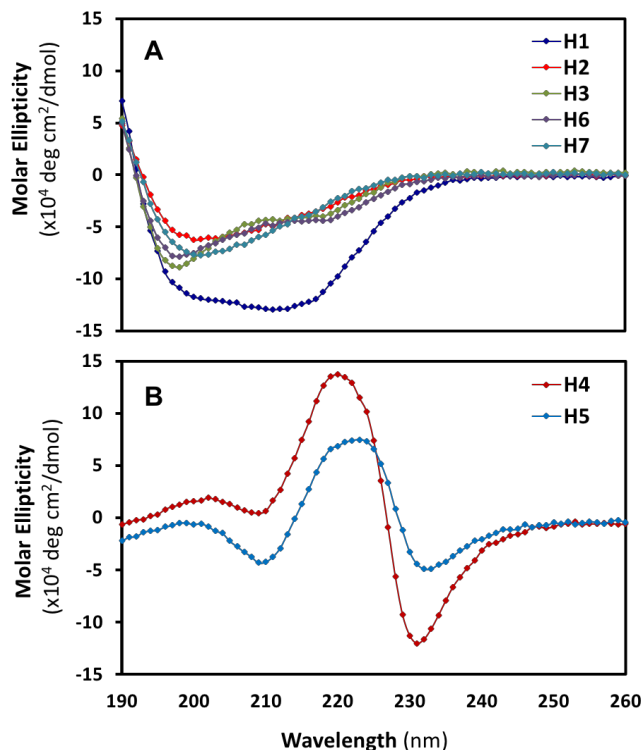
Figure S3. CD spectra of peptoid pentamers indicating that some hetero-oligomers adopt a conformational preference in solution. Comparison of CD spectra of **(A)** chiral phenyl-containing peptoids (**H1**, **H2**, **H3**, **H6** and **H7**) and **(B)** chiral naphthyl-containing peptoids (**H4** and **H5**) shows that the identity of the bulky chiral sidechain directly affects the CD signal. All peptoids were analyzed at 50 µM in 10 mM sodium phosphate buffer, pH 7.5 at 25 °C. In the case of naphthyl-containing peptoids (**H4** and **H5**, Figure S2B), CD spectra resemble those of homo-oligomer poly-*N*s1npe tetramer.[1] An intense minimum around 230 nm and a broad maximum near 215 nm suggest a helical conformation for these hetero-peptides. Fuller et. al. assigned the minima at 231 nm to the overlap of naphthalene units as *i* and *i* + 3 residues in the peptoid helix.[2] The CD of **H4** describes a potentially more structurally restricted ensemble than **H5**.
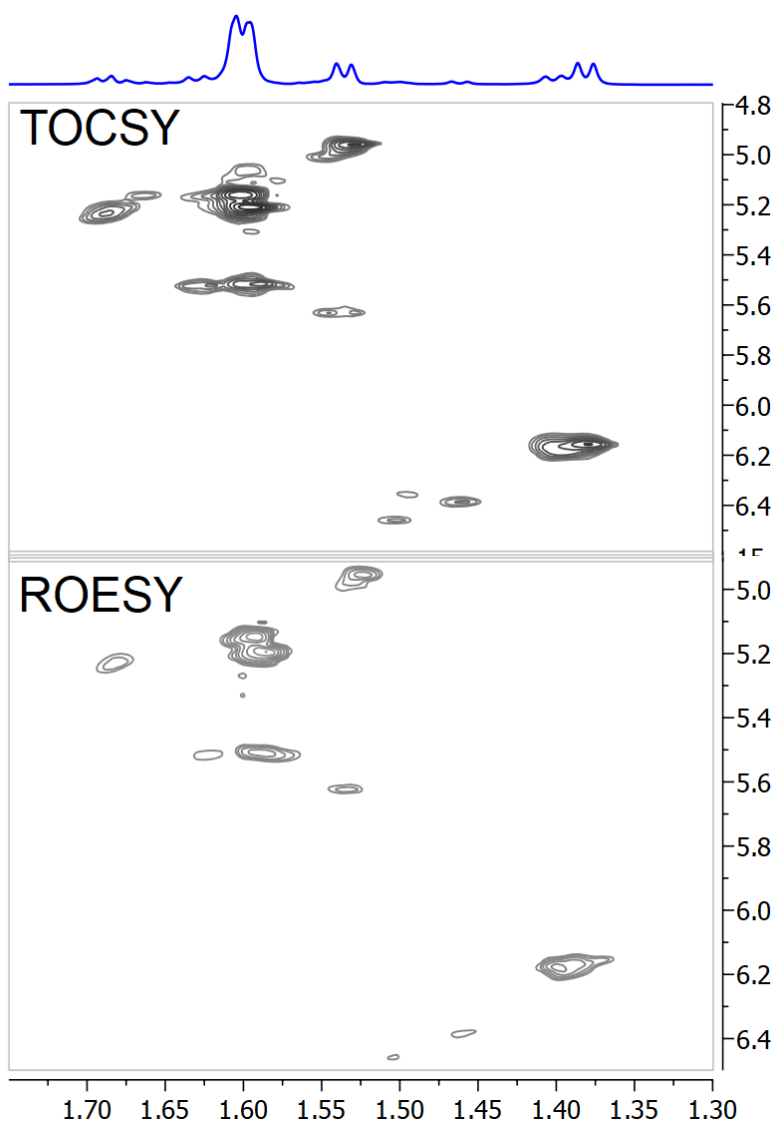
Figure S4. 2D NMR results (Top: TOCSY, Bottom: ROESY) of purified **H4** peptoid show the existence of multiple conformers. The two methyl groups on the chiral naphthyl rings produce multiple resonances in the methyl region (1.30-1.75 ppm) indicating the presence of multiple conformers instead of a single, well-defined conformation. Spectral deconvolution of the **H4** methyl resonances indicates two main conformers, one with overlapping methyl peaks at 1.6 ppm and the second with resonances at 1.54 ppm and 1.37 ppm. Based on the chemical shift range and the TOCSY cross-peaks from methyl groups the resonances in the 5.3 to 6.5 ppm range correspond to the CH groups in the naphthyl side chains.
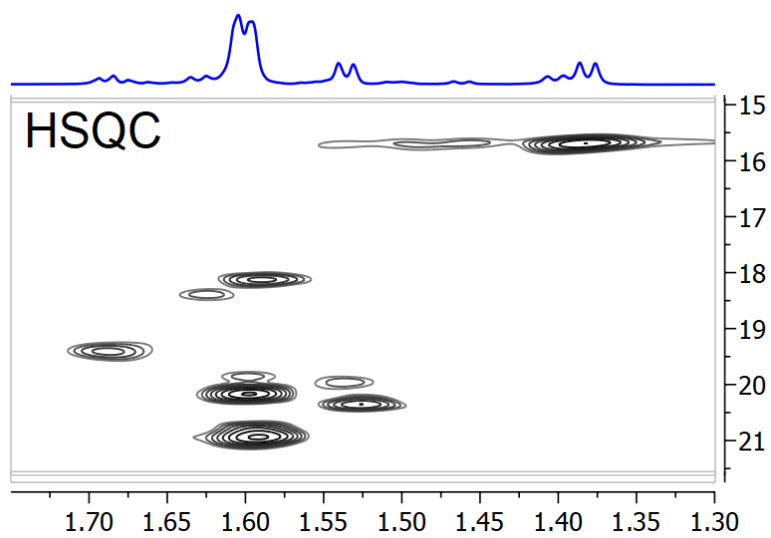
Figure S5. 2D (HSQC) NMR results show agreement with ROESY and TOCSY spectra regarding multiple **H4** peptoid conformers.
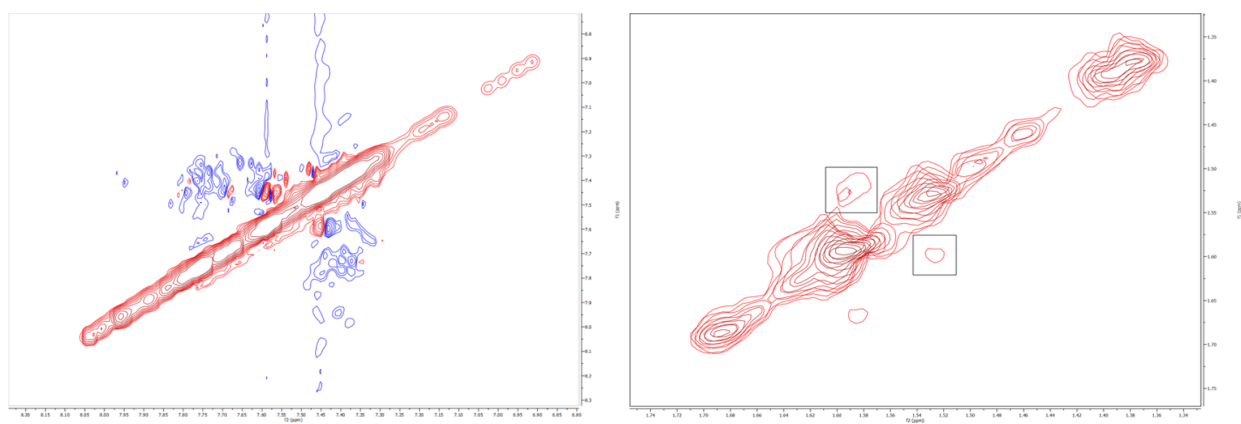
Figure S6. ROESY spectra of the aromatic region (left) and methyl region (right) for peptoid **H4**. Cross-peaks within black boxes represent exchange cross-peaks between methyl protons in the two conformers.

Figure S7. ^{1}H and ^{13}C NMR for peptoid **H1**.

Figure S8. ^{1}H and ^{13}C NMR for peptoid **H2**.

Figure S9. ^{1}H and ^{13}C NMR for peptoid **H3**.

13

Figure S10. ^{1}H and ^{13}C NMR for peptoid **H4**.

Figure S11. ^{1}H and ^{13}C NMR for peptoid **H5**.

Figure S12. ^{1}H and ^{13}C NMR for peptoid **H6**.

Figure S13. ^1H and ^{13}C NMR for peptoid **H7**.

Figure S14. ^{1}H and ^{13}C NMR for peptoid **H8**.
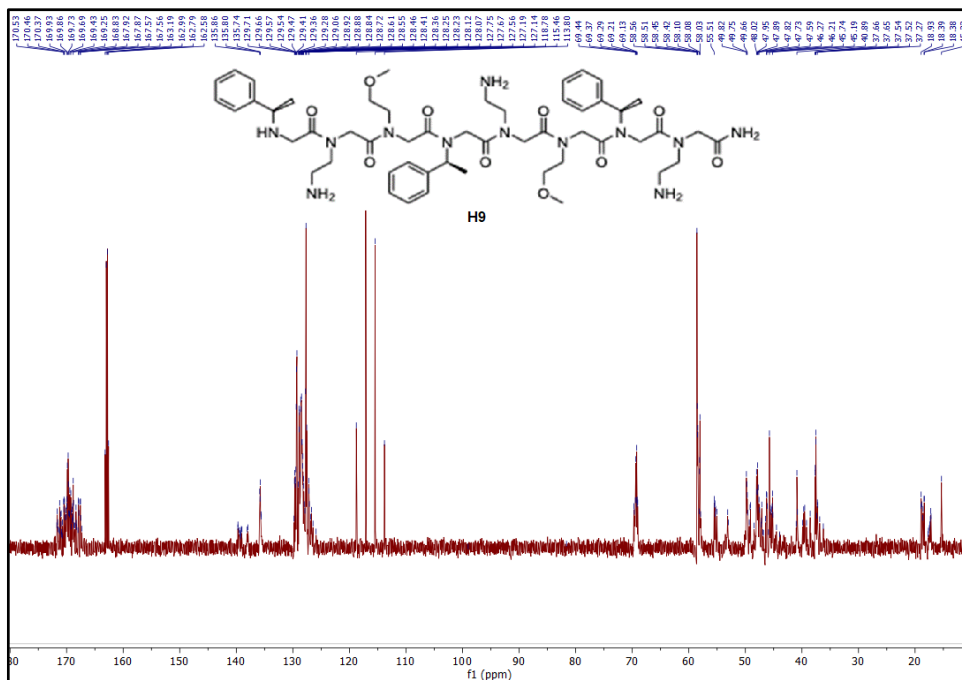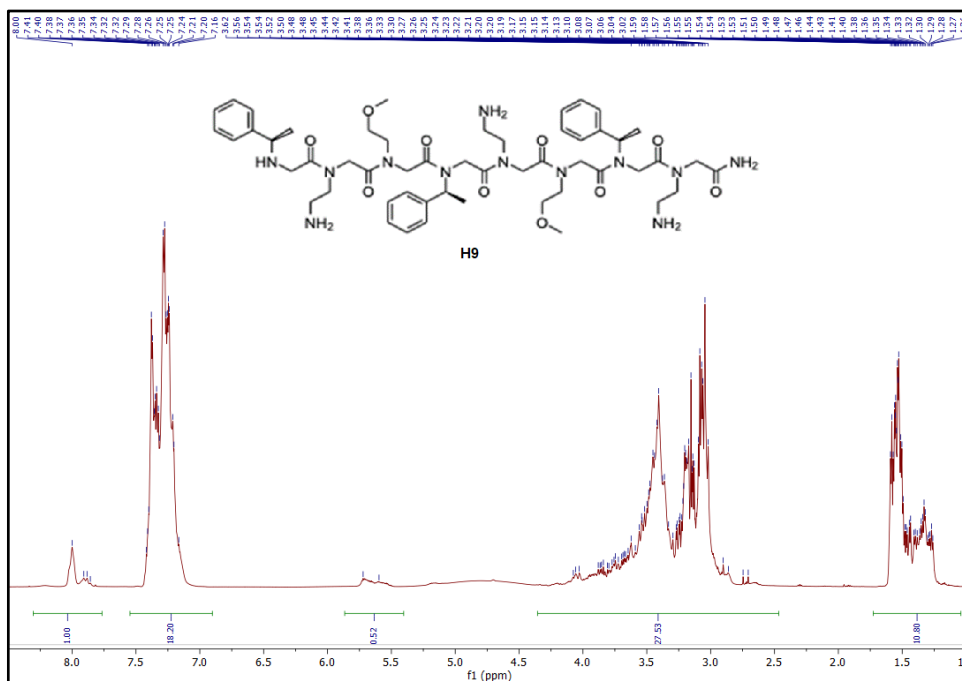
Figure S15. ^{1}H and ^{13}C NMR for peptoid **H9**.

NMR data supports a limited number of conformations

We employed NMR to determine the occupancies of distinguishable conformational motifs. This contrasts with how NMR is normally employed, where peaks are assigned, and through-space coupling provides distance information leading to determination of a structure. However, in complex mixtures it is nearly always the case that NMR peaks can be observed but not assigned. Even so, critical information can be found in the spectra. When conformational motifs comprise the majority of signal, we can partition these into states and determine an occupancy ratio. Thus, we can estimate the occupancy of certain conformers.

We focused our attention on the methyl region of the TOCSY and ROESY spectra (Fig. 2 and Figs. S4-S6), corresponding to the two methyl groups on the chiral naphthyl rings, which is the least congested and most straightforward to interpret within the spectra. From Figure S4 we are able to resolve 16 total cross peaks in the CH-CH3 region. Given two cross peaks per conformer, we conclude that there are 8 total conformers represented in the TOCSY or ROESY spectra. Spectral deconvolution of the **H4** methyl resonances indicates two main conformers exist, one with overlapping methyl peaks at 1.6 ppm and the second with resonances at 1.54 ppm and 1.37 ppm (Figure 2B), accounting for approximately 80% of the total intensity (e.g. 80% of the total conformers in solution). Through-space magnetization (CH-CH3 cross-peaks) shows both conformers exist simultaneously based on opposite-sign cross peaks (Fig. 2B). We then examined the CH region of the spectra and observed exchange cross peaks corresponding to the same CH resonances identified from CH-CH3 ROESY cross peaks (Fig. 2A), suggesting that the two conformers are long lived on NMR timescales and interconverting. We note that while the observed ROESY intensity for the two major conformers was 80% of the total, in the 1D NMR spectra those conformers represent 65% of the total intensity. This difference is consistent with the small fractions represented by several of the conformers (as deduced from 1D deconvolution) not being observed in the ROESY spectra with lower signal to noise. Thus, while in the TOCSY and ROESY spectra we are able to deconvolve 8 conformers, within the 1D spectra, which has a better signal-to-noise ratio, additional low occupancy conformers appear. Utilizing spectral deconvolution of 1D spectra for peptoid **H4** we obtained approximately 24 doublets (Fig. S10), which would correspond to 12 different conformational states; most of them present in very small quantities (amplitudes).

Coupled with modeling, we used NMR to assess the occupancy of conformers and not for specific structural assignment, as is most typical. As such, we present below our additional points of analysis that guided our assignment and conclusions. First, the observability of any cross-peak in the 2D TOCSY or

ROESY spectra clearly indicates a conformational state is well occupied and long-lived on NMR timescale (Fig. 2 & Fig. S4 – S6).   Hence, we have a means to identify the existence of major conformational preferences when they exist. Further, we note that confirmation that these major conformers are correctly identified as two states, comes from observing exchange cross-peaks within the ROESY spectrum. For example, one concern in ROESY experiments is that TOCSY artifacts can appear as ROESY cross peaks if the cross peaks are J coupled and close in space. We eliminated that potential artifact by focusing on ROESY cross-peaks for protons not coupled to each other (not exhibiting TOCSY peaks). Further, since the CH groups in any given conformer cannot be coupled (there are too many bonds in between them) there is no possibility of TOCSY artifacts contributing to ROSEY for these exchange cross-peaks. Thus, we find that the exchange cross-peaks observed for the CH resonances of the naphthyl side chain indicate exchange between two conformers in which the CH moiety assumes different positions in a given conformer. Going further to determine structures of these populated conformers is not possible because the spectra are too congested to allow peak assignment.

Second, we considered but rejected other potential data analysis pitfalls, for example if whether unassignable peaks are actually impurities. Reasonably, this is extremely unlikely because the peptoid was highly purified and because we observe exchange cross peaks between the major conformers.

Third, we note that we focused on the exchange cross peaks presented above, and not others, as from analysis of those presented above (CH-CH3) we can unequivocally demonstrate exchange. Assignment of additional exchange cross-peaks is frustrated because most are unobservable due to a combination of factors: 1) the exchange rate is outside of the range of the experimental modality, 2) overlapping spectra, 3) too close to the diagonal, or 4) below the signal-to-noise threshold. However, the presence or absence of these exchange peaks does not change our analysis since we can simply count the largest peaks and put a lower-bound on the minimum fraction of the total population. Thus, we only examined the subset of the corroborating exchange peaks, which were clearly identifiable as exchange peaks and not artifacts (note the comments above on our elimination of TOCSY artifacts in the ROESY analysis).

Fourth, we considered another potential data analysis pitfall for example, we questioned why the exchange for one naphthyl side chain is observed and presented in Figure 2A, but not the other quasi-symmetric naphthyl side chain.   One possible explanation for this is that the chemical shift differences are not the same. A large chemical shift difference for one naphthyl does not prevent the other naphthyl from having a small chemical shift difference, and thus the second naphthyl side-chain would have a cross-peak too close to the diagonal to be observed clearly. This is plausible for a stacked conformer where one

chiral center (CH group of naphthyl) is within the ring current field of the second naphthyl (thus contributing to a significant resonance shift), while the second chiral center is outside of the stacked rings and experiences a minimal change in chemical shift. While there may be additional explanations possible, of the possible scenarios here we do not see any that would alter our inferences from the observations.

Computational Details

Methods. Computational modeling of the **H4** peptoid used Rosetta3 modeling software [version 2018.18][3]. A monomeric structure for the residue *Nae* was generated using Gaussian 09[4] and a backbone-dependent torsional library was generated using the Rosetta make_rot_lib protocol[5]. The other residues in the **H4** peptoid were already represented in the Rosetta peptoid residue database. All **H4** conformations are generated using a RosettaScripts XML file, which conducts the following operations:

1) Initialize a conformation of **H4** using all five residues and randomize all except the -dihedrals, which are initialized to 180°.
2) Relax side chains (with the backbone fixed) by sampling 100 alternative rotamers to find the most energetically-favored conformations.
3) Relax the full **H4** conformation using a single-pass of gradient-descent with an exact line search (the -dihedrals move only slightly; always less than 30°).
4) Save this configuration and repeat steps $1 - 4$, 10^5 times.

From the ensemble of 10^5 conformers, the 20% lowest-energy conformers are considered (Rosetta score values less than -10 REU based on the REF2015 score function)[6]. We group these by structural similarity into clusters (using *g_cluster* in GROMACS ver. 4.5.5.[7] with a cutoff of 1 Å RMSD). Despite the mostly random initialization, the relaxation process drove the low energy conformations to within 1 Å RMSD for 99% of the ensemble. In this convergence group we analyzed fine-details of residue-residue pairings and discovered a clear naphthyl-naphthyl stacking interaction, characteristic of the principal cluster's centroid (Figure S16).
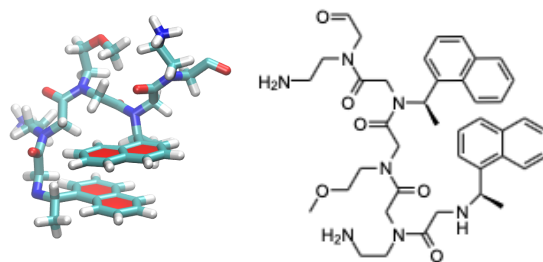
Figure S16. The principal cluster centroid shows clear naphthyl-naphthyl stacking. The average naphthyl-naphthyl distance of this structure is 4.4 Å. Of the low-energy states, 99% were within 1 Å RMSD of this conformation. While that still allows conformations with unstacked naphthyls, these had no single representative pattern that could be easily displayed.

Based on this observation, we defined an order parameter for naphthyl-naphthyl stacking, which compared distances between each six-membered ring using a method first described for RNA nucleobases and urea molecules[8]. A center is determined for the proximal (P) and distal (D) rings (Figure S17) of each naphthyl residue based on the coordinates of three ring atoms in each (1, 3, 4a, 6, 8 in Figure S17). Taking the pairwise distances between these center points gives distances of P to P, and D to D, and an average of the two values for each **H4** conformation.
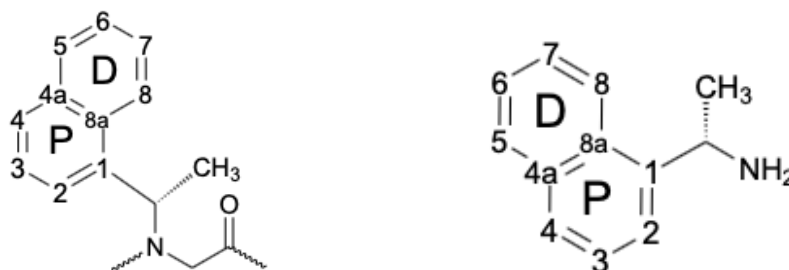
Figure S17. The proximal ring (P) and distal ring (D) of each naphthyl group of the Ns1npe monomer (left) and submonomer (right). The pairwise distances between the same rings in residues 1 and 4 of the **H4** peptoid can be calculated using methods previously employed to describe stacking between nucleobases in RNA and urea molecules.[8] The three atoms used to define the center of each six-membered ring are 2, 4 and 8a for P, and 5, 7 and 8a for D.

The naphthyl-naphthyl distances for all **H4** conformers can be used to determine the prevalence of the different naphthyl-naphthyl stacking interactions. In this way, we determine an enumerable set of conformers in the original ensemble and the ensemble of lowest energy conformers. A bimodal distribution of conformers emerges in both ensembles, with an inflection point near 6 Å for all three calculated naphthyl-naphthyl distances (Figure S18). Values above this cutoff are identified as 'unstacked' and those below it are identified as 'stacked'.

In the original ensemble of 10^5 conformers, 18.5% of the ensemble occupies the peak below the 6 Å cutoff, but in the lower-energy ensemble the relative occupancy of this peak increases to 26.52%.
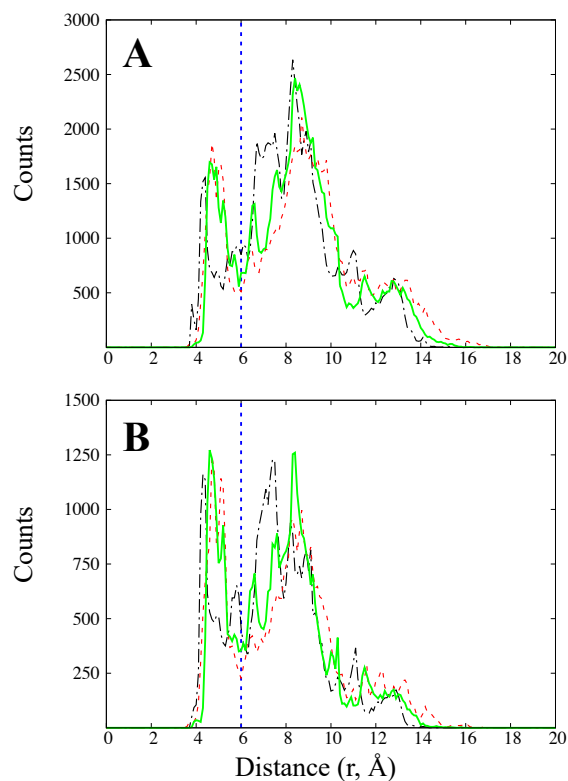
Figure S18. Naphthyl-naphthyl distances show a few preferred conformations when all ω angles are initialized to 180° before minimization. The complete ensemble of 10^5 conformations is shown in **(A)**, and the subset of the 20000 lowest-energy conformers is shown in **(B)**. The blue line at 6 Å represents the cutoff for ring stacking based on the inflection point, and from previous ring stacking calculations[7]. Three pairwise distances are shown: proximal-proximal (black), distal-distal (red), and the 'average' of both distances (green). Strong peaks are shown within the stacking cutoff (3 – 6 Å) for all three calculations, and a second prominent peak is shown in the range 6 – 10 Å.

A serendipitous accident in our initial modeling revealed an important principle of peptoid organization. In the Rosetta version used in this paper it was discovered that Rosetta incorrectly assigns flexibility to the -dihedrals in peptoids. Our conformations correctly incorporate this strong bias when initialized to 180° since the bonds do not vary more than 30° during the conformational energy relaxation (line minimization).

It is interesting to compare these results to our initially incorrect calculations in which most ω-dihedrals were allowed to vary over the full 360° range, and at random, some ω-dihedrals might have been set to 180°. When we take the 20% lowest-energy conformers from this ensemble, and cluster by structural

similarity, we find that the most representative structure (Figure S19) is extended, with a naphthyl-naphthyl distance ~10.3 Å.
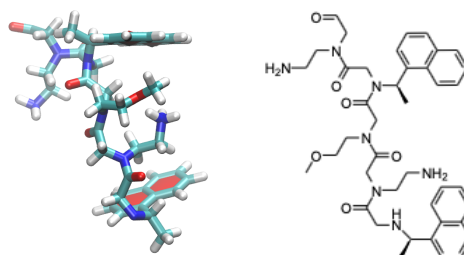
Figure S19. When the bias on the ω-dihedrals is removed (incorrectly), the cluster centroid shows an extended conformation with no naphthyl-naphthyl stacking. The average naphthyl-naphthyl distance is over 10 Å. Of the low-energy states, over 90% came within 1 Å RMSD of this conformation.

Surprisingly, the preferred stacked arrangement, evidenced by the peak in the ensemble with all ω-dihedrals initialized to 180° (Figure S18) vanishes if the ω-dihedral angles are allowed more conformational freedom. This can be seen in Figure S20, which shows a broad unimodal distribution spanning the entire range of naphthyl-naphthyl distances for **H4**.
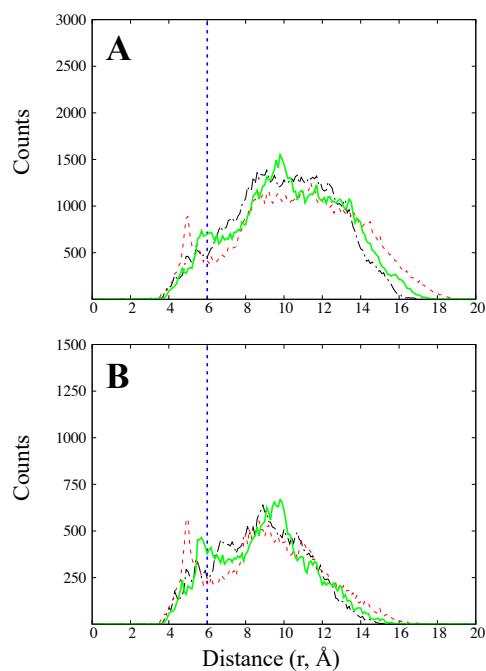
Figure S20. Naphthyl-naphthyl distances show a unimodal distribution when -dihedrals are incorrectly allowed more flexibility and only a few are ever set to 180° before minimization. A vestigial weak peak at short distance is likely attributable to that modest bias. Three pairwise distances – proximal-proximal (black), distal-distal (red), and

the 'average' of both distances (green) – are shown.   The complete ensemble of 10^5 conformations is shown in **(A)**, and the subset of the 20000 lowest-energy conformers is shown in **(B)**.

A protocol, effectively-equivalent to our initialization of ω-dihedrals to 180°, will likely be incorporated into a future version of Rosetta for further studies of peptoid modeling.

References:

1) Zuckermann, R. N.; Kerr, J. M.; Kent, S. B. H.; Moos, W. H. *J. Am. Chem. Soc.* **1992**, *114* (26), 10646-10647.
2) Figliozzi, G. M.; Goldsmith, R.; Ng, S. C.; Banville, S. C.; Zuckermann, R. N. *Methods in Enzymology*, Academic Press: 1996; Vol. 267, pp 437-447.
3) Leaver-Fay, A.; Tyka, M.; Lewis, S. M.; Lange, O. F.; Thompson, J.; Jacak, R.; Kaufman, K.; Renfrew, P. D.; Smith, C. A.; Sheffler, W.; et al. Rosetta3: An Object-Oriented Software Suite for the Simulation and Design of Macromolecules. *Methods Enzymol.* **2011**, *487* (C), 545–574.
4) Frisch, M. J.; Trucks, G. W.; Schlegel, H. B.; Scuseria, G. E.; Robb, M. A.; Cheeseman, J. R.; Scalmani, G.; Barone, V.; Mennucci, B.; Petersson, G. A.; Nakatsuji, H.; Caricato, M.; Li, X.; Hratchian, H. P.; Izmaylov, A. F.; Bloino, J.; Zheng, G.; Sonnenberg, J. L.; Hada, M.; Ehara, M.; Toyota, K.; Fukuda, R.; Hasegawa, J.; Ishida, M.; Nakajima, T.; Honda, Y.; Kitao, O.; Nakai, H.; Vreven, T.; Montgomery, J. A., Jr.; Peralta, J. E.; Ogliaro, F.; Bearpark, M.; Heyd, J. J.; Brothers, E.; Kudin, K. N.; Staroverov, V. N.; Kobayashi, R.; Normand, J.; Raghavachari, K.; Rendell, A.; Burant, J. C.; Iyengar, S. S.; Tomasi, J.; Cossi, M.; Rega, N.; Millam, J. M.; Klene, M.; Knox, J. E.; Cross, J. B.; Bakken, V.; Adamo, C.; Jaramillo, J.; Gomperts, R.; Stratmann, R. E.; Yazyev, O.; Austin, A. J.; Cammi, R.; Pomelli, C.; Ochterski, J. W.; Martin, R. L.; Morokuma, K.; Zakrzewski, V. G.; Voth, G. A.; Salvador, P.; Dannenberg, J. J.; Dapprich, S.; Daniels, A. D.; Farkas, Ö.; Foresman, J. B.; Ortiz, J. V.; Cioslowski, J.; Fox, D. J. Gaussian 09 Revision E.01, **2009**.
5) Renfrew, P. D.; Craven, T. W.; Butterfoss, G. L.; Kirshenbaum, K.; Bonneau, R. A Rotamer Library to Enable Modeling and Design of Peptoid Foldamers. *J. Am. Chem. Soc.* **2014**, *136* (24), 8772–8782.
6) Park, H.; Bradley, P.; Greisen, P.; Liu, Y.; Mulligan, V. K. Simultaneous Optimization of Biomolecular Energy Functions on Features from Small Molecules and Macromolecules. **2016**.
7) Pronk, S.; Páll, S.; Schulz, R.; Larsson, P.; Bjelkmar, P.; Apostolov, R.; Shirts, M. R.; Smith, J. C.; Kasson, P. M.; van der Spoel, D.; et al. GROMACS 4.5: A High-Throughput and Highly Parallel Open Source Molecular Simulation Toolkit. *Bioinformatics* **2013**, *29* (7), 845–854.
8) Miner, J. C.; García, A. E. Equilibrium Denaturation and Preferential Interactions of an RNA Tetraloop with Urea. *J. Phys. Chem. B* **2017**, *121* (15), 3734–3746.